

Thick Filament Length and Isoform Composition Determine Self-Organized Contractile Units in Actomyosin Bundles

Todd Thoresen,[†] Martin Lenz,^{‡§¶} and Margaret L. Gardel^{†‡§*}

[†]Institute for Biophysical Dynamics, [‡]James Franck Institute, and [§]Department of Physics, University of Chicago, Chicago, Illinois; and

[¶]Laboratoire de Physique Théorique et Modèles Statistiques, CNRS and Université Paris-Sud, Bâtiment 100, Orsay Cedex, France

ABSTRACT Diverse myosin II isoforms regulate contractility of actomyosin bundles in disparate physiological processes by variations in both motor mechanochemistry and the extent to which motors are clustered into thick filaments. Although the role of mechanochemistry is well appreciated, the extent to which thick filament length regulates actomyosin contractility is unknown. Here, we study the contractility of minimal actomyosin bundles formed *in vitro* by mixtures of F-actin and thick filaments of nonmuscle, smooth, and skeletal muscle myosin isoforms with varied length. Diverse myosin II isoforms guide the self-organization of distinct contractile units within *in vitro* bundles with shortening rates similar to those of *in vivo* myofibrils and stress fibers. The tendency to form contractile units increases with the thick filament length, resulting in a bundle shortening rate proportional to the length of constituent myosin thick filament. We develop a model that describes our data, providing a framework in which to understand how diverse myosin II isoforms regulate the contractile behaviors of disordered actomyosin bundles found in muscle and nonmuscle cells. These experiments provide insight into physiological processes that use dynamic regulation of thick filament length, such as smooth muscle contraction.

INTRODUCTION

Actomyosin contraction is ubiquitous among muscle and nonmuscle cells in eukaryotic organisms as a mechanism to generate tension and drive morphological changes at the subcellular, cellular, and tissue length scales. Filaments of actin and myosin II are highly conserved constituents of contractile bundles used in cell migration (1,2), cell division (3,4), skeletal and smooth muscle contraction (5,6), and tissue morphogenesis (7). A myriad of regulatory proteins, actin- and myosin-binding proteins as well as varied myosin II isoforms guide the self-organization of contractile actomyosin bundles with distinct architectures to form the cytokinetic contractile ring (4), stress fibers (2), and graded polarity bundles (2) in nonmuscle cells as well as smooth and striated myofibrils. Such varied architectures and compositions are expected to guide the transmission of actomyosin forces generated at molecular length scales to cellular length scales and to optimize the contractile forces and shortening rates of bundles used for diverse physiological processes.

In striated myofibrils, actomyosin is organized into highly ordered structures known as sarcomeres, which has facilitated our understanding of contractility over the past ~60 years (8). Myosin II is a dimer of trimers that contains two identical motor domains, or heads, at the N-terminus of each heavy chain and a C-terminal tail that regulates its assembly into elongated thick filaments (9). In sarcomeres, bipolar thick filaments of skeletal muscle myosin are segregated toward the pointed end of F-actin, whereas cross-linkers are located at the F-actin barbed ends. Upon

stimulation of motor activity, the myosin motor heads generate tension of F-actin and drive F-actin translocation to increase the extent of thick and thin (F-actin) filament overlap. Here, maximum contraction speed under zero load is then determined by the motor-mediated F-actin gliding velocity v_0 to obtain myofibril shortening rates of $1\text{--}2\text{ s}^{-1}$ (5,10). The maximum extent of contraction is determined by the change in overlap between thick and thin filaments (~30%), whereas the maximal tension is determined by the number of myosin heads engaged on the F-actin (5). Thus, sarcomeres serve as fundamental contractile units that drive striated myofibril contraction. Due to geometrical constraints of the sarcomere, the contractile properties of striated muscle are largely invariant (5), but can occur through changes in motor head cycling through thin filament regulation (5).

In contrast, actomyosin bundles in myofibrils of smooth muscle cells and nonmuscle cells are highly disordered but more versatile, supporting contraction over a large range of strains, speeds, and tension. For instance, the rate of smooth muscle contraction varies significantly from $0.02\text{--}0.25\text{ s}^{-1}$ (6,11–13) up to strains of nearly 100%. In nonmuscle cells, ~100% changes in length are also common during morphological changes and exhibit maximal shortening rates of 0.004 s^{-1} in the contractile ring (4) and $0.02\text{--}0.08\text{ s}^{-1}$ in stress fibers (14,15). These contractile properties are thought to arise from contractile units within the bundles, but the identification of such has proven challenging due to their highly disorganized nature (4,11). In smooth muscle, regulation of shortening rates is believed to occur by dynamic regulation of myosin ATPase activity (16), the existence of a myosin latch state (12) or changes in the myosin thick filament length and organization

Submitted July 25, 2012, and accepted for publication December 21, 2012.

*Correspondence: gardel@uchicago.edu

Editor: James Sellers.

© 2013 by the Biophysical Society
0006-3495/13/02/0655/11 \$2.00



<http://dx.doi.org/10.1016/j.bpj.2012.12.042>

(17,18). Thus, changes in both myosin motor mechanochemistry and thick filament length are likely to be important in regulation of contraction. However, a common framework in which to understand contraction of disordered actomyosin bundles in these diverse tissue types is unknown.

To identify general mechanisms regulating contraction in nonsarcomeric actomyosin bundles, we have developed an *in vitro* model of actomyosin bundle contractility. We previously demonstrated that bundles composed of F-actin and smooth muscle myosin (SMM) thick filaments spontaneously assemble contractile units with a well-defined force-velocity relationship (19). In this work, we show that bundles of F-actin formed with either nonmuscle or skeletal muscle myosin thick filaments also self-organize into contractile units with distinct unloaded shortening velocities and maximum tensions. To identify the role of thick filament length in the regulation of contractility, we varied the average number of motor heads per thick filament while maintaining similar myosin motor and F-actin densities within the bundle. We found that the maximum tension, unloaded shortening rate, and extent of contraction are all directly proportional to the thick filament length. These results are in good agreement with a model where disordered actomyosin bundles spontaneously form a series of contractile units whose stall force is determined by that of the number of motor domains within a single thick filament and unloaded velocity is determined by the motor gliding speed. Moreover, our results show that larger thick filaments promote the formation of contractile units with higher frequency along the bundle, leading to changes in the shortening rate for bundles formed with identical myosin isoforms but varied thick filament length. The inverse relationship between thick filament and contractile unit length we observe is consistent with our recently developed model on the formation of contractile units through F-actin buckling by myosin-generated stresses (20). These results elucidate how myosin thick filament length and isoform composition regulate the contractility of disordered actomyosin bundles found in diverse cellular processes.

MATERIALS AND METHODS

Buffers

Myosin Storage Buffer

50 mM HEPES, pH 7.6, 0.5 M KCl, 1 mM DTT.

Myosin Spin-Down Buffer

20 mM MOPS, pH 7.4, 500 mM KCl, 4 mM MgCl₂, 0.1 mM EGTA, 500 μM ATP.

G-actin Buffer (G-Buffer)

2 mM Tris-HCl, pH 8.0, 0.2 mM ATP, 0.2 mM CaCl₂, 0.2 mM DTT, 0.005% NaN₃.

F-actin Buffer (F-Buffer)

10 mM imidazole, pH 7.0, 1 mM MgCl₂, 50 mM KCl, 2 mM EGTA.

Bead Wash Buffer

20 mM MOPS, pH 7.4, 50 mM KCl, 4 mM MgCl₂, 0.1 mM EGTA.

Assay Buffer

20 mM MOPS, pH 7.4, 4 mM MgCl₂, 0.1 mM EGTA, 0.7% methylcellulose, 0.25 mg/ml glucose, 0.25% β-ME, 0.25 mg/ml glucose oxidase, 35 μg/ml catalase. KCl and ATP are also included in Assay Buffer and adjusted as described below for different thick filament preparations and to stimulate contraction. KCl concentration is always at 100 mM KCl during the final wash step after bundle formation and during contraction.

Protein preparations

Protocols, as previously described in (19), were used to obtain purified SMM from chicken gizzard and nonmuscle myosin (NMM) from expired human platelets obtained at a local blood bank. The purified NMM and SMM was then phosphorylated by myosin light chain kinase isolated from turkey gizzard, purified, and administered as described (21), and labeled with Oregon Green maleimide dye as previously described (19). Skeletal myosin (SkM) was purchased from (Cytoskeleton, Inc., Denver, CO) and also similarly labeled with Oregon Green maleimide dye. All fluorescent myosin preparations had an average of ~2 dye labels per heavy chain. Fluorescently labeled myosin was snap-frozen in liquid nitrogen, aliquoted in Storage Buffer, and stored at -80°C. Unlabeled myosin was stored at either -80°C (SkM) or in liquid nitrogen (NMM and SMM) in Myosin Storage Buffer. Actin was purified from acetone powder (Pel-Freez Biologicals, Rogers, AR) as previously described (22) and stored in G-Buffer. Biotinylated actin was prepared using the EZ-Link NHS-PEO₄ biotinylation kit (Thermo Scientific, Hanover, IL). All myosin concentrations were determined by using an extinction coefficient of 0.56 ml mg⁻¹ cm⁻¹ (280 nm) and 0.76 ml mg⁻¹ cm⁻¹ (498 nm). All myosin concentrations are reported in terms of single motors, or one half of a myosin hexamer.

Actin filament assembly and characterization

Before polymerization with F-buffer, biotinylated actin was mixed with unlabeled actin in a 1:10 stoichiometry. Actin filaments were then polymerized by adding 1/10 volume of 10× F-buffer to a solution containing G-actin that also included 1 mM ATP. Tetramethyl rhodamine phalloidin (Cytoskeleton) was then added in a 1:2 molar ratio (phalloidin:G-actin). The F-actin lengths were determined by fluorescence imaging and we would expect these lengths to be exponentially distributed, as seen in previous measurements.

Myosin thick filament assembly and characterization

Before thick filament formation, fluorescently labeled and unlabeled myosin hexamers were mixed such that a 6–10 μM myosin solution contained 20% labeled hexamer. To isolate the active myosin species, the solution mixture was then subject to separation by F-actin affinity in Myosin Spin-Down buffer containing 0.5 mM ATP, as previously described (19). The supernatant was then dialyzed against 50 mL of Storage Buffer that also contained 0.2 mM EGTA for 2 h using a membrane filter (0.025 μm VSWP, Millipore, Billerica, MA) floating on the buffer surface with gentle stirring to remove excess nucleotide. The myosin solution was then subject to particular conditions to obtain myosin filaments with length *L* as follows: 1), SkM, *L* = 1.5 μm: rapid dilution to 1 μM in Assay Buffer

adjusted to a final concentration of 100 mM KCl and 45 min incubation on ice; 2), SkM, $L = 1.0 \mu\text{m}$: rapid dilution to 1 μM in Assay Buffer adjusted to 150 mM KCl final concentration and 45 min incubation on ice; 3), SkM, $L = 0.6 \mu\text{m}$: rapid dilution to 1 μM in Assay Buffer adjusted to 200 mM KCl and 45 min incubation on ice; 4), SMM, $L = 1.2 \mu\text{m}$: 2 h dialysis against Myosin Storage Buffer adjusted to 100 mM KCl, followed by the dilution of the myosin to 1 μM in Assay Buffer adjusted to 100 mM KCl; 5), SMM, $L = 0.7 \mu\text{m}$: 2 h dialysis against Myosin Storage Buffer adjusted to 200 mM KCl, followed by the dilution of the myosin to 1 μM with Assay Buffer adjusted to 200 mM KCl, final; 6), SMM, $L = 0.2 \mu\text{m}$: rapid dilution to 1 μM in Assay Buffer adjusted to 200 mM KCl and 45 min incubation on ice; 7), NMM: rapid dilution to 1 μM in Assay Buffer adjusted to 100 mM KCl final concentration and 45 min incubation on ice.

The lengths for skeletal and smooth muscle myosin thick filaments were determined by quantitative analysis of fluorescent images of myosin thick filaments, which had an extended rod-like appearance and whose lengths were above the diffraction limit of our light microscope. The lengths were obtained by measuring the lengths of >50 myosin puncta. In the case of the shortest smooth muscle filament ($L = 0.2 \mu\text{m}$), the length was determined in fluorescence images by the ratio of integrated filament intensity of the small filament (I_{small}) to that of a larger filament (I_{large}) where length (L_{large}) was measured directly such that $L_{\text{small}} = (I_{\text{small}}/I_{\text{large}})L_{\text{large}}$. All measurements of filament lengths were also confirmed with transmission electron microscopy of negatively stained samples. Our measurements are consistent with previously reported smooth and skeletal thick filament lengths measured by dynamic light scattering and electron microscopy (23) (see Table 2).

Bundle assembly and contraction

Assembly of actomyosin bundles took place in a custom flow chamber as previously described (19). Briefly, the steps were: 1), incubation of 1 μM 10% biotinylated F-actin with neutravidin beads conjugated to the surface of a biotinylated polyacrylamide gel for 30 min. 2), Extensive perfusion of Assay Buffer (adjusted to KCl concentration used for thick filament assembly). Most, but not all, F-actin in solution was removed at this time. 3), Perfusion of 1 μM of filamentous myosin in ATP-free Assay Buffer (adjusted to KCl concentration used for thick filament formation) and 30 min incubation to allow for bundle formation by myosin-mediated cross-linking of actin filaments bound to beads and in solution. 4), Wash with ATP-free Assay Buffer, adjusted to 100 mM KCl. 5), Perfusion of Assay Buffer adjusted to 100 mM KCl and containing 1 mM ATP. Contraction of SkM and NMM bundles was initiated with Assay Buffer that contained 1 mM ATP, whereas contraction of SkM bundles was initiated with Assay Buffer that either contained 0.1 or 1 mM ATP, with no discernible differences detected between the two ATP concentrations. Steps 4 and 5 were performed quickly (within several minutes); all contraction was performed in Assay Buffer containing 100 mM KCl. The methylcellulose contained within the Assay buffer was used primarily to increase viscosity of the surrounding solution to permit imaging; it was not sufficient to induce bundling in the absence of myosin thick filaments and nor required for either myosin-mediated bundle assembly or contraction (data not shown).

Imaging

A customized flow chamber was used from Chamli Live Cell imaging (Quorum Technologies, Inc., Guelph, Canada). Fluorescence imaging was performed using a Ti-E microscope body (Nikon, Melville, NY) fitted with a CSU-X spinning disc confocal head (Yokogawa, Japan), a HQ2 CoolSnap CCD camera (Roper Scientific, Tuscan, AZ) or Evolve 512 EMCCD camera (Photometrics, Tuscan, AZ) with the electron multiplier gain set to half maximum, and a $60\times 1.2\text{NA}$ water immersion objective

lens (Nikon). The instrument was controlled with Metamorph software (MDS Analytical Technologies, Sunnyvale, CA). Velocity data for NMM was collected at 1 Hz, whereas velocity data for SMM and SkM actomyosin contractions were collected at 0.2 and 10 Hz, respectively.

Image analysis and force measurements

All details of quantitative image analysis can be found in our previous manuscript (19). In brief, quantitative fluorescence imaging was used to determine bundle composition by analyzing F-actin or myosin images acquired using the same laser power and acquisition settings and corrected for photobleaching. To determine the average fluorescence signal in the bundle, the average intensity of a transverse line scan across an F-actin or actomyosin bundle averaged over a 5–10 μm length of the bundle was determined, corrected for photobleaching, and background subtracted. To quantify the actin and myosin within bundles, the intensity of actin and myosin in the bundle was compared to intensity of individual F-actin and myosin puncta (presumed to be thick filaments) bound to a glass coverslip or gel surface. Transverse line scans across individual F-actin, myosin puncta, or bundles all yielded a Gaussian-like profile. The number of F-actin per bundle cross section was determined by comparing the background-subtracted peak intensity of transverse line scans across filaments on the surface of a glass coverslip, to that across a bundle. Images of F-actin and bundles were acquired on the same day using the same phalloidin-actin stock to ensure identical labeling density. A more rigorous explanation on the determination of F-actin and myosin density, and mole ratios of myosin and actin within bundles ($R_{\text{M:A}}$) was described previously (19).

Beads were affixed to a sufficiently compliant polyacrylamide gel such that deformations occur upon bundle contraction and result in bead displacement. Calibration of the bead displacement into a tensile force was performed as previously described (19). In brief, the effective spring constant for polyacrylamide gels of different stiffness was determined by traction force microscopy methods (described in detail in Fig. S6 of (19)). Due to the random geometry of the experimental system, a subset of bundles spanning suitably attached bead pairs were selected for further analysis; beads with multiple bundles attached or observed to rotate upon contraction were excluded. The bead displacement measured after the contraction completed relative to the initial position was calculated and then converted to a force using the effective spring constant. Due to differences in the magnitude of tension generated by bundles formed with different myosin thick filament lengths, the shear elastic modulus G' of the polyacrylamide gel varied for each particular filament preparation as follows: $G' = 54 \text{ Pa}$ (SkM, $L = 0.2 \mu\text{m}$ and NMM), $G' = 280 \text{ Pa}$ (SMM, $L = 0.6$ and $0.7 \mu\text{m}$ and SkM $L = 1.5 \mu\text{m}$), and $G' = 600 \text{ Pa}$ (SkM, $L = 1.0$ and $1.5 \mu\text{m}$, and SMM $L = 1.2 \mu\text{m}$). The recipes used to obtain polyacrylamide gels of these stiffnesses were previously described (24,25). We confirmed that the maximum force generated was independent of the stiffness of the polyacrylamide gel (Fig. S4 in the Supporting Material).

Measurement of bundle lengths and shortening velocities

Measurements of bundle lengths were determined by manually measuring the contour lengths of a bundle using the multisegment tool in Metamorph (MDS). We explored the contraction velocity as a function of sampling frequency to identify and to minimize effects observed at low acquisition rates, in which the bundle contraction rate slows during the sampling interval, or at high acquisition rates, in which insufficient bundle contraction during the sampling interval resulted in a noise dominated measurement (Fig. S2). The maximum sampling rate possible with our imaging setup was 10 Hz. We found the optimal acquisition sampling rates amenable to our imaging setup for each myosin isoform: 10 Hz for SkM and 1 Hz for NMM. 0.2 Hz was chosen for SMM to allow for direct comparison in

previous work (19). We note that our optimal sampling rate for SkM bundles was at the maximum permitted by our imaging setup and thus, measurements of contraction speeds for these bundles may be impacted by undersampling effects and underestimate the actual speeds.

Determination of number of heads per thick filament

The number of motor heads per thick filament for skeletal myosin was estimated from a recent model of filament structure that contains a linear density of myosin heads (23). Other skeletal constructs were assumed to scale with length, with a central bare zone length held constant at 150 nm. Smooth muscle linear densities of 4 molecules per 14.5 nm were taken from (26). Because the filament lengths we measured for NMM were consistent with previous measurements (27), we presumed the same number of motor heads, 56, found in this previous work.

RESULTS

Diverse myosin II isoforms drive contractility of reconstituted actomyosin bundles

We previously showed that bundles comprised of F-actin and a sufficiently high density of SMM thick filaments spontaneously self-organize contractile units that drive bundle contraction and tension generation (19). To determine if this is a generic behavior of F-actin and myosin II, we compared the contractile properties of bundles formed with similar densities of skeletal muscle, smooth muscle, or nonmuscle myosin. Each of these myosin isoforms has distinct mechanochemistry, which alters the speed of F-actin translocation in gliding filament assays (Table 1). In addition, differences in the tail regions of the heavy chain regulate the assembly of thick filaments with distinct geometries and lengths (Table 1). In vivo, SkM and NMM assemble into bipolar thick filaments composed of several hundred and tens of myosin dimers, respectively (Table 1). By contrast, SMM forms side-polar thick filaments that can contain from 100 to >800 motors (Table 1). In vitro, thick filament polymerization occurs by diluting or dialyzing full-length motor proteins stored at 0.5 M KCl to physiological salt concentrations (0.1–0.2 M KCl). Under these conditions, the average number of myosin motor domains per thick filament \bar{N}_{heads} is $\bar{N}_{heads} = 56$ for NMM, $\bar{N}_{heads} = 373$ for SMM, and $\bar{N}_{heads} = 576$ for skeletal muscle myosin (Table 2).

TABLE 2 Lengths of myosin thick filaments (Mean \pm SD) under different preparation conditions, as measured by fluorescence and electron microscopy ($n = 100$ for fluorescence microscopy, $n = 20$ for transmission electron microscopy measurements)




Thick filament preparation	Thick filament length		# of motor heads
	Fluorescent microscopy	Electron microscopy	
SkM, 100 mM KCl, dilution	1.45 \pm 0.20 μ m	1.34 \pm 0.28 μ m	576
SkM, 150 mM KCl, dilution	0.96 \pm 0.14 μ m	0.71 \pm 0.20 μ m	308
SkM, 200 mM KCl, dilution	0.63 \pm 0.11 μ m	0.47 \pm 0.11 μ m	184
SMM, 100 mM KCl, dialysis	1.20 \pm 0.26 μ m	0.86 \pm 0.19 μ m	624
SMM, 200 mM KCl, dialysis	0.71 \pm 0.16 μ m	0.61 \pm 0.18 μ m	373
SMM, 200 mM KCl, dilution	0.19 \pm 0.05 μ m ^a	0.21 \pm 0.06 μ m	98
NMM, 100 mM, dilution	N.D.	0.23 \pm 0.07 μ m	56

^aThe length of this condition was determined in fluorescence images by comparing the integrated intensity to one where a direct length measurement was possible; details in Materials and Methods. The number of motor heads for each construct was determined by linear density of SkM (23) and SMM (26) and based on a previous measurement for NMM (27).

Actomyosin bundles are formed so that their ends are attached to streptavidin beads bound to the surface of a compliant polyacrylamide gel to facilitate contraction and tension measurements (19). F-actin asters are first formed by incubating biotinylated F-actin of length $\sim 5 \mu$ m with surface-bound streptavidin beads and washing extensively with Assay Buffer to remove most, but not all, F-actin (Fig. 1 A). A solution of 1 μ M myosin thick filaments in ATP-free Assay Buffer is then perfused into the flow chamber to promote cross-linking between F-actin asters and the small amount of F-actin remaining in solution to form bundles. Within minutes after myosin thick filament addition, a stable network of curved and branched actomyosin bundles suspended above the gel surface is formed. The flow cell is then washed to remove any unbound myosin from solution with ATP-free Assay Buffer (Fig. 1 A).

Because both the myosin and the F-actin in the sample are fluorescently labeled, quantitative fluorescence imaging is used to directly assess bundle organization and composition

TABLE 1 Comparison of motor mechanochemistry and thick filament geometry of myosin II isoforms

	Nonmuscle	Smooth muscle	Skeletal muscle
			
Motor speed, v_0	0.1–0.3 μ m/s (37,38)	0.4–>0.7 μ m/s (37,39)	5–6 μ m/s (39)
Motor stall force, f_{stall}	Est. ~ 2 pN	~ 1.4 pN (40)	~ 1.4 –4 pN (40,41)
Thick filament geometry	Bipolar	Side polar	Bipolar
Thick filament length	$\sim 0.3 \mu$ m (27)	~ 0.3 –1.5 μ m (26,42)	1.5 μ m (23)
# motors/filament, \bar{N}_{heads}	56 (40)	200–>800 (42,43)	~ 600 (23)

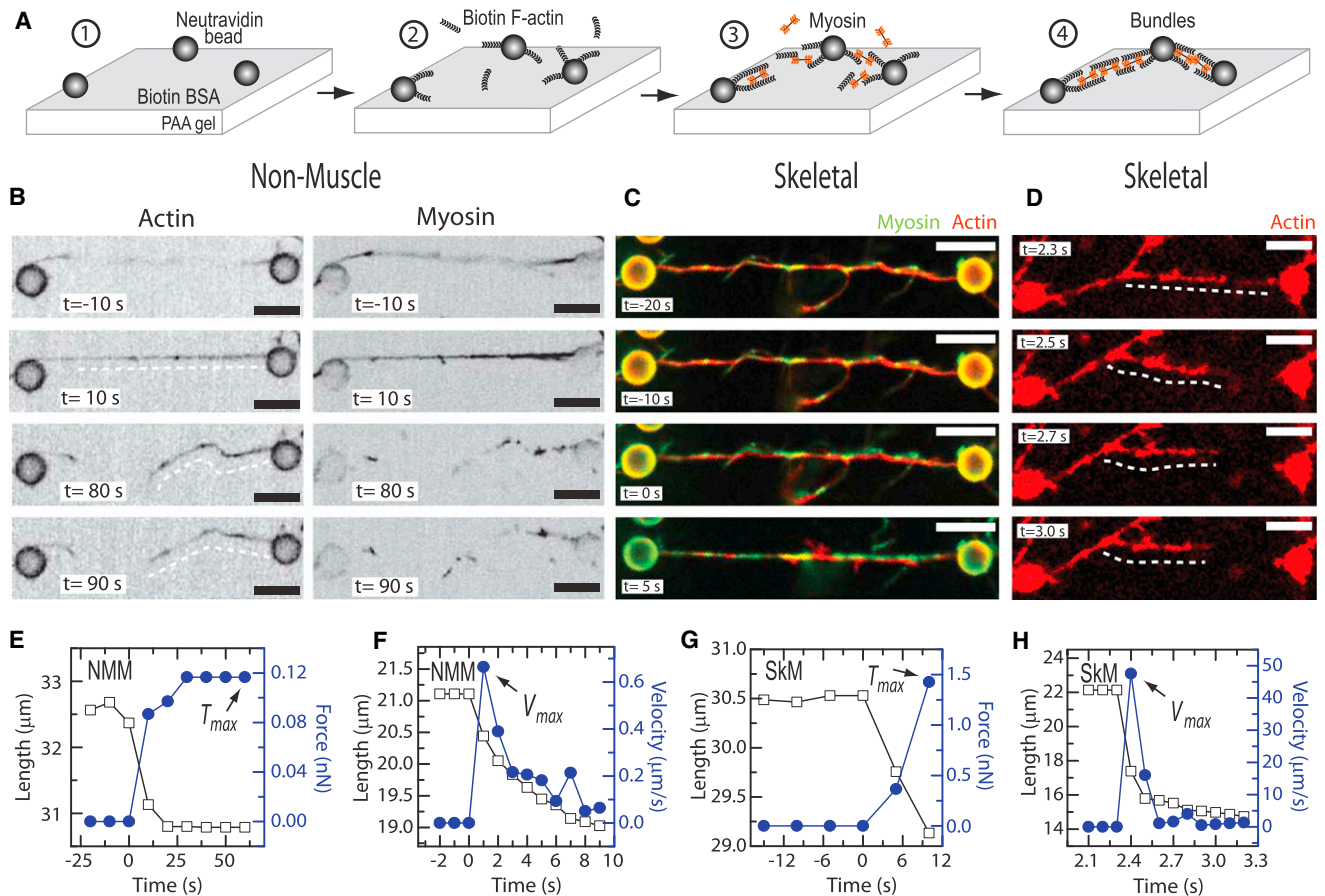


FIGURE 1 Assembly and measurements on reconstituted actomyosin bundles. (A) Schematic describing assembly of templated actomyosin bundles on a polyacrylamide gel substrate performed in the following four steps. 1) Neutravidin beads are bound to a biotinylated-BSA-coated polyacrylamide gel surface. 2) Biotinylated F-actin binds to the beads forming F-actin asters. 3) Myosin thick filaments are introduced into ATP-free Assay Buffer. 4) After ~30 min incubation, actomyosin bundles form near the surface that span between beads. Free myosin filaments in solution are washed out with Assay Buffer, followed by perfusion of Assay Buffer containing 1 mM ATP, which induces motor activity and allows bundles to contract. (B) Montage of inverted contrast images of actin (left) and a nonmuscle myosin (right) bundle as contraction occurs after ATP addition ($t = 0$ s). At $t = 70$ s, the bundle ruptures and the untensed bundle contracts further. (C) Montage of a contracting skeletal actomyosin bundle with the first image ($t = -20$ s) as an overlay of actin and myosin images. Upon perfusion of ATP ($t = 0$ s) the bundle begins to contract. (D) Montage of a skeletal actomyosin bundle after a rupture event where the bundle continues to contract when tension is released. White dashed line indicates the contour length of the shortening bundle. (E) Graph indicating the shortening of the bundle contour length and tension buildup over time for the nonmuscle bundle shown in (B). (F) Graph indicating the shortening and the shortening rate of an unloaded nonmuscle bundle over time. (G) Graph indicating the shortening of the bundle contour length and tension buildup over time for the skeletal bundle shown in (C). (H) Graph indicating the shortening and the shortening rate of a skeletal bundle after rupture relieves bundle tension. Arrows in (E–H) indicate either the maximal unloaded shortening velocity immediately after bundle rupture (V_{max}), or maximal bundle tension (T_{max}). All scale bars indicate 5 μm . Images in (B–D) are inverse contrast, and have been subject to low-pass filtering for clarity.

(19). Myosin decorates F-actin all along the bundle length, with no significant density variations or distinct organization (Fig. S1). In all cases, the bundle lengths range from ~5 to ≥ 30 μm , longer than individual F-actin, and contains ~4 F-actin per cross section (Fig. 2A). The mole ratios of myosin heavy chains/actin ($R_{M:A}$) are similar between different isoforms (Fig. 2B) and are ≥ 1 , above the threshold we previously determined necessary to support contractility (19).

Upon the perfusion of Assay Buffer containing 1 mM ATP, the bundle contour lengths shorten so that they become straight and taut (Fig. 1, B–D, Movie S1 and Movie S2). Because the elastic modulus of the gel to which beads are

firmly affixed is known, bead displacement in the direction of contraction directly reflects tension generated by the actomyosin bundle (19). Tension buildup within the bundles increases concurrently with bundle shortening, until a maximal tension T_{max} is achieved and contraction stops (Fig. 1, E and G). The time scales for contraction vary greatly between myosin isoforms. For bundles formed with skeletal muscle myosin, tension buildup occurs over < 10 s (Movie S2), whereas those formed with NMM take longer than 30 s (Movie S1).

After building tension, many of the bundles subsequently rupture, creating untethered bundles that continue

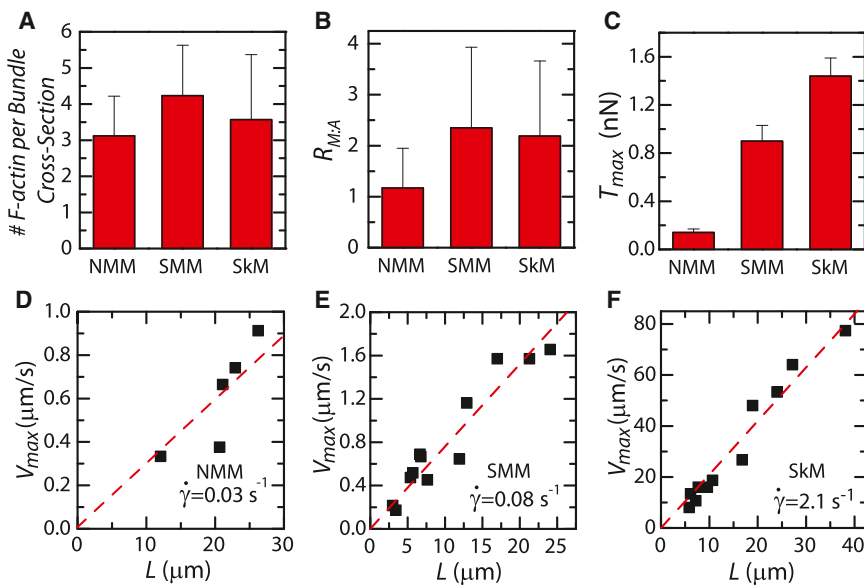


FIGURE 2 Contractile properties of bundles formed with $1 \mu\text{M}$ of nonmuscle (NMM), smooth (SMM), or skeletal (SkM) myosin II isoforms. (A–C) Thick filaments are formed under conditions such that the mean number of motor heads $\bar{N}_{heads} = 56$ (NMM, left), 373 (SMM, center), and 576 (SkM, right). (A) Quantity of F-actin per bundle cross section for bundles formed with NMM, SMM, or SkM. (B) Mole ratio of myosin heavy chain/G-actin ($R_{M:A}$) for bundles formed with $1 \mu\text{M}$ of NMM, SMM, or SkM. (C) Maximum tension T_{max} built by bundles formed with three different myosin isoforms. (D–F) Maximum unloaded shortening velocity as a function of initial bundle length for (D) NMM, (E) SMM, and (F) SkM. Data for individual bundles are indicated by black squares. Dashed line is a linear fit to the data with slope a measure of the unloaded shortening strain rate $\dot{\gamma}$, which is indicated at the bottom right of each graph. Data in A and B reflect mean \pm SD for $n = 20$ for NMM, SMM, and SkM bundles.

to contract under zero external load. Differences in the incidence of these bundle ruptures are observed and appear to be isoform dependent (Fig. S5 and Fig. S6). The unloaded contraction speed is initially highest after rupture and then subsequently slows down and ultimately stops (Fig. 1, F and H, Fig. S2).

Myosin II isoform specificity of self-organized contractile units

Our *in vitro* assay permits the construction of actomyosin bundles formed from different myosin isoforms with similar density of F-actin and myosin II that appear by light microscopy to be highly disorganized (Fig. 2, A and B, Fig. S1). This permits us to isolate the extent to which motor isoform and thick filament architecture regulate contractility. The maximal tension T_{max} built by different myosin isoforms varies dramatically; bundles formed with NMM generate low tension, ~ 100 pN, whereas those formed with skeletal muscle myosin generate large tensions, ~ 1.4 nN (Fig. 2 C). Tension built by bundles formed with SMM is ~ 0.8 nN (19). In all cases, no strong correlation between maximum tension and bundle length is observed (Fig. S4).

The maximal unloaded bundle contraction speed V_{max} is proportional to the bundle length L for bundles formed with NMM (Fig. 2 D), SMM (Fig. 2 E), and skeletal muscle myosin (Fig. 2 F). Such telescopic contraction reflects a well-defined bundle shortening rate $\dot{\gamma} = V_{max}/L$ that is independent of overall bundle length. The measured shortening rate for bundles formed with skeletal muscle myosin is 2.1 s^{-1} , which is significantly larger than those formed with smooth muscle (0.08 s^{-1}) or nonmuscle myosin (0.03 s^{-1}) (Fig. 2, D–F). Due to limitations of our imaging setup, our measured contraction rate for SkM bundles is

likely impacted by effects of undersampling and is likely an underestimate of the actual contraction speed (Fig. S2).

The bundle length-independent maximal tension and length-dependent shortening velocity reflect the self-organization of reconstituted actomyosin bundles into a series of contractile units along the bundle, a phenomenon we described previously for SMM (19). Although no apparent structural characteristic of contractile units exists in these disordered bundles, the simplest picture of such a unit would be at least one thick filament facilitating sliding and tension on antiparallel F-actin. Linking several units in series would yield a shortening rate $\dot{\gamma} = v_0/\ell_0$ where v_0 is the unloaded motor gliding speed and ℓ_0 is the contractile unit length. Differences in the myosin gliding speed between SkM, SMM, and NMM isoforms would account for a ~ 10 -fold difference in unloaded shortening rates (Table 1). However, we observe a difference of an unloaded bundle shortening rate of 100-fold (Fig. 2, D–F). This implies that thick filament length may also play an important role in regulating the contractile unit length ℓ_0 .

Bundle tension and unloaded contraction rate are proportional to thick filament length

The length of thick filaments can be controlled *in vitro* by altering the formation conditions of thick filament preparations. For example, smooth muscle filaments can adopt much longer lengths by limiting the rates of filament nucleation and promoting the rates of filament elongation by slowly lowering ionic strengths through dialysis (28). Conversely, myosin filament lengths can be reduced to $0.2 \mu\text{m}$ by rapid dilution into 200 mM KCl. By modifying the thick filament assembly conditions, we vary the average lengths of SMM thick filaments from 0.2 to $1.2 \mu\text{m}$ (Table 2, Fig S3). Using the known linear density of myosin heads,

this results in thick filaments where the number of motor heads \bar{N}_{heads} varies from ~ 100 to ~ 600 . Similar modifications to skeletal muscle myosin thick filament length can be made by modifications to the preparation conditions (29) (Table 2, Fig. S3).

Actomyosin bundles are formed as described in Fig. 1, but with $1 \mu\text{M}$ SMM assembled into thick filaments with a variable number of motor heads \bar{N}_{heads} . Importantly, changes to \bar{N}_{heads} did not have an effect on either the quantity of F-actin or the density of myosin that was present in the bundles (Fig. 3, A and B). After formation, bundles are washed with Assay Buffer adjusted to 100 mM KCl to maintain identical buffer conditions for contraction. Thus, our assay permits direct comparison between bundles formed with identical densities of F-actin and SMM motors with the only difference being the extent to which motors are clustered into thick filaments.

In all conditions where \bar{N}_{heads} is altered, contraction is observed but the maximum tension and shortening rate change significantly. The maximum tension T_{max} increases from 0.5 nN for $\bar{N}_{heads} = 200$ to 2.0 nN for $\bar{N}_{heads} = 600$ (Fig. 3 C), reflecting the increased number of motor heads acting in parallel on F-actin with increased thick filament length. Consistent with increased tension buildup, the incidence of bundle rupture also increases with \bar{N}_{heads} (Fig. S5). These effects on tension and rupture incidence are also observed in bundles formed with skeletal muscle myosin thick filaments of varying length (Fig. S6).

The unloaded shortening velocity is proportional to bundle length for all conditions (Fig. 2, D–F, Fig. S5, A and B, Fig. S6 A), emphasizing the robustness of telescopic contraction in self-organized actomyosin bundles. Quite surprisingly, we find a strong linear dependence in the unloaded contraction rate as a function of myosin thick filament length (Fig. 3 D). As \bar{N}_{heads} increases from ~ 100 to ~ 600 , the unloaded shortening rate increases from 0.02 to 0.12 s^{-1} . The linear dependence on the unloaded shortening rate as a function of thick filament length is also observed for bundles formed with skeletal muscle myosin (Fig. 4).

Mechanical model reveals length and properties of contractile units

Our data show that diverse myosin II isoforms support telescopic contractility of reconstituted actomyosin bundles. Across these conditions, the F-actin lengths as well as F-actin and myosin density within the bundle remain constant. Thus, altered contractile properties arise solely from differences in motor mechanochemistry and the extent of motor clustering into thick filaments. The telescopic contraction observed over all conditions indicates we can model the bundle as a series of mechanical units of length ℓ_0 that contract with a maximal speed v_{max} and generate a maximal tension of F_{stall} (Fig. 4 A). We note that, in these self-

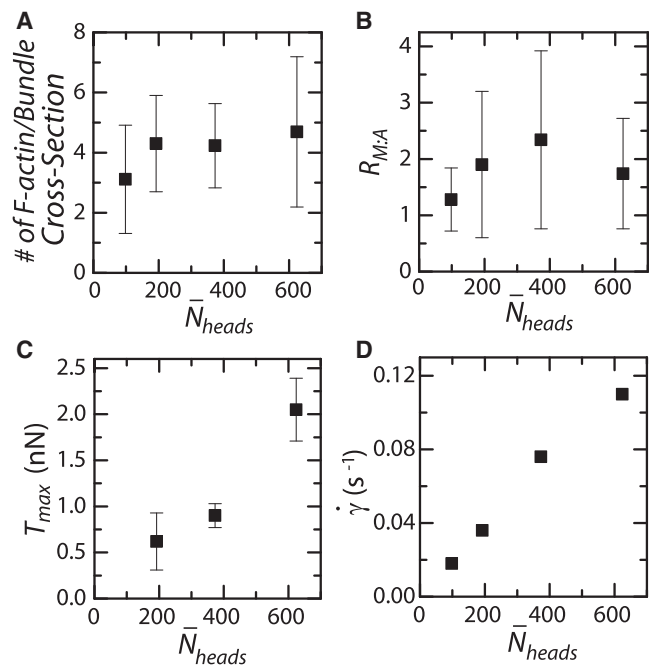


FIGURE 3 Contractile properties regulated by thick filament size. All data shown are from bundles formed with $1 \mu\text{M}$ SMM that is assembled into filaments with a different number of motor heads per filament (N_{heads}) by altering myosin thick filament assembly conditions. (A) Quantity of F-actin per bundle cross section as \bar{N}_{heads} is varied. (B) The mole ratio of myosin heavy chains/G-actin $R_{M:A}$ as a function of \bar{N}_{heads} . (C) Maximum tension, T_{max} , generated by bundles as a function of \bar{N}_{heads} . (D) Unloaded shortening rate $\dot{\gamma}$ as a function of \bar{N}_{heads} . In (A and B), data reflect mean \pm SD for $n = 20$ bundles for all four conditions ($\bar{N}_{heads} = 98, 192, 373, \text{ and } 624$). In (C), data reflect mean \pm SD for $n \geq 5$. Strain rates obtained from linear fits to data shown in Fig. 2, Fig. S5, Fig. S6 and from previously published data (19).

organized bundles, there is no evident structural manifestation of the contractile unit (e.g., sarcomeric organization). Thus, the schematic in Fig. 4 A serves only to illustrate the mechanical elements of our model and should not be used to infer their structural origin.

Due to the geometrical arrangement of contractile units, the maximal tension T_{max} generated by the bundle is independent of bundle length, as we observe experimentally, and reflects the maximum force generated (or stall force) of each contractile unit such that $T_{max} = F_{stall}$. As the number of myosin heads per thick filament is varied, the F_{stall} of each thick filament will also change such that $F_{stall} \sim N_{heads} f_{stall}$ where f_{stall} is the stall force of an individual myosin motor domain. Our data show that, across all three myosin isoforms, the bundle tension is directly proportional to the number of motor heads per thick filament N_{heads} (Fig. 4 B). The slope of this line yields a proportionality of $f_{stall} = 2.9 \text{ pN}$, consistent with reported stall forces of myosin II (Table 1). Thus, a contractile element likely corresponds to a single myosin thick filament, which is reasonable given the small number of F-actin ($\sim 2\text{--}4$) per bundle cross section.

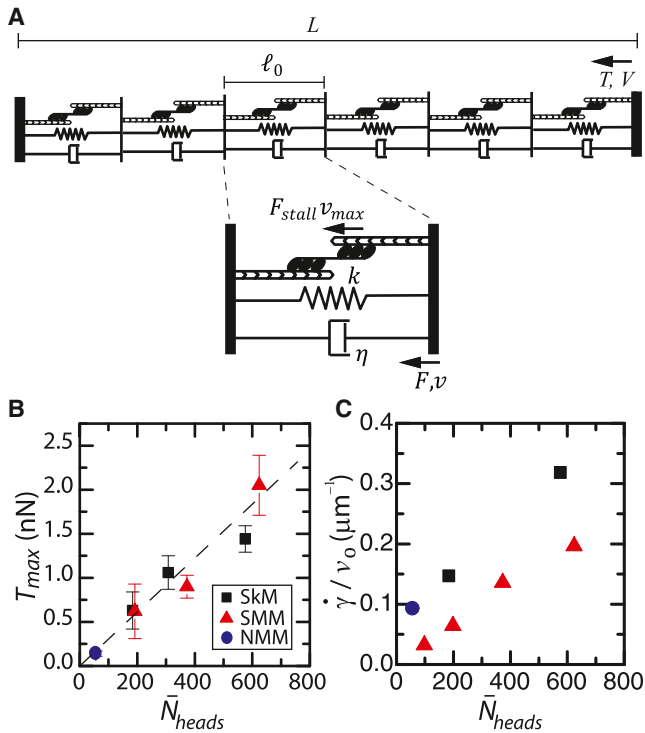


FIGURE 4 Stall forces and contraction rates are dependent on the number of motors per filament. (A) Schematic model illustrating the mechanical elements in the model described in the main text. Contractile units of length ℓ_0 are linked in series within a bundle of length L . Tension T and bundle shortening velocity V are characterized for an entire bundle. F_{stall} and v_0 are the motor stall forces and gliding motor velocities for the myosin isoform within an individual contractile unit. The viscoelastic response of the bundle is captured by an elastic spring with spring constant k in parallel with viscous dashpot η to reflect internal friction. Unlike a sarcomere, these mechanical elements have no clear structural analogs in the disordered actomyosin bundles studied in this work. (B) Experimentally measured bundle tension plotted as a function of the average number of motor heads per filament for SkM, SMM, and NMM data. Linear fit to the slope indicates a common stall force per head of 2.9 pN. Data are plotted as mean \pm SD $n \geq 5$. (C) The contraction rate, or strain rate, for each myosin isoform construct is normalized by their respective unloaded velocities, and then plotted as a function of the number of heads per filament.

The unloaded shortening rate of the bundle is $\dot{\gamma} = v_{max}/\ell_0$, which reflects the maximal velocity of each unit divided by its length. Because these bundles are highly disordered, there is no clear structure to determine the contractile unit length or organization. Moreover, the disordered nature of the bundles may result in a shortening rate that is dominated by internal friction and dissipation within the bundle (captured by the friction element η). Thus, the regulation of shortening rates is not immediately obvious. Naively, one might presume that the number of contractile units formed would be proportional to the number of thick filaments. If this were true then, as N_{heads} increased, the overall thick filament density would decrease (and ℓ_0 would increase) to result in a reduced bundle shortening rate. Instead, we find that the shortening rate is proportional to

the thick filament length, or $\dot{\gamma} \propto N_{heads}$. The changes in shortening rate observed in Fig. 2, D–F, and Fig. 3 D could arise from changes in v_{max} , ℓ_0 , or both.

To elucidate the underlying physical mechanisms controlling bundle contractility, we developed a mechanical model of an individual contractile unit. Each contractile unit contains an element that reflects the contractile motor activity placed in parallel with the viscoelastic response of the bundle, captured by an elastic spring with spring constant k in parallel with a viscous dashpot with friction coefficient η to reflect internal friction (Fig. 4 A) (30). The microscopic origins of these parameters arise from the complex protein-protein interactions within the bundle. For instance, k may arise from cross-linking effects of myosin II motors, whereas η could arise from frictional drag between neighboring F-actin or lubrication flows of fluid within the bundle. The parallel arrangement of k and η accommodates for the constant and finite bundle length observed at long times after rupture. To account for the contractile tension generated by myosin thick filaments, we use a linearized force-velocity relationship (30): $F_m(v) = F_{stall}(1 - v/v_0)$ where v_0 is the unloaded thick filament gliding speed and F_{stall} is the stall force of the thick filament where $F_{stall} = N_{heads} f_{stall}$.

We consider the strain γ of the mechanical units at zero load where all internal forces within this unit must balance such that

$$0 = -\eta \frac{d\gamma}{dt} - k\gamma - F_m, \quad (1)$$

and the shortening rate is $\dot{\gamma} = d\gamma/dt = -v/\ell_0$. The solution to this differential equation yields $\gamma(t) = F_{stall}/k (1 - e^{-t/\tau})$ where the relaxation time constant $\tau = \eta_e/k$ is determined by an effective viscosity

$$\eta_e = \eta + F_{stall}\ell_0/v_0, \quad (2)$$

that reflects both the contributions viscous/frictional drag determined by the properties of motor proteins themselves ($F_{stall}\ell_0/v_0$) as well as other sources of drag within the bundle (η). The unloaded shortening speed of the contractile unit is then determined by $v = F_{stall}\ell_0/\eta_e$.

Eq. 2 delineates two asymptotic regimes for bundle contraction. If $\eta \gg F_{stall}\ell_0/v_0$, internal friction within the bundle dominates and the motor is operating near stall throughout contraction and $\dot{\gamma} = F_{stall}/\eta$. However, our experiments show that different myosin isoforms with similar F_{stall} have dramatically different shortening rates (e.g., for $N_{heads} = 200$, $\dot{\gamma} = 0.04 \text{ s}^{-1}$ for SMM, and $\dot{\gamma} = 0.97 \text{ s}^{-1}$ for SkM) suggesting that this drag is not dominant. On the other hand, if $\eta \ll F_{stall}\ell_0/v_0$, then dissipation within the bundle is small and does not significantly affect the rate of F-actin translocation by myosin. Here, the maximum shortening rate is $\dot{\gamma} = v_0/\ell_0$. We find that when the shortening rates for skeletal and smooth muscle myosin

are normalized by the motor gliding speed v_0 , the two isoforms yield a similar value $\dot{\gamma}/v_0 \sim 0.05 - 0.15$ for $\bar{N}_{heads} = 200$ (Fig. 4 C). This indicates the initial shortening rate of our bundles is, in fact, near the unloaded regime of motor sliding such that $\eta_e \approx F_{stall}\ell_0/v_0$. This argument suggests that similarly sized thick filaments self-organize into contractile units with similar length, despite differences in the unloaded gliding speed. The discrepancy in scaling between data sets may reflect inherent noise in our measurements, contribution of internal drag, or other effects not considered by our simplistic model.

To determine the origin of changes in the shortening rate as a function of thick filament length, N_{heads} , we consider experiments performed with varied thick filament length where we observe that $\dot{\gamma} \propto N_{heads}$ (Fig. 3 D). Because $\dot{\gamma} = v_0/\ell_0$ and v_0 are constant, this indicates that ℓ_0 must vary inversely with thick filament length such that $\ell_0 \propto 1/N_{heads}$. Thus, as the thick filament length increases, the frequency of forming contractile units also increases and their effective length ℓ_0 decreases. This is quite a surprising result. Forming larger thick filaments increases the propensity to form contractile units, even though the overall density of thick filaments decreases. Thus, the self-organized contractile units are quite different than that of sarcomeres, where a constant fraction of thick filaments is attributed to a contractile unit. Instead, a force-dependent self-organization process within the disordered bundle likely dominates.

DISCUSSION

Here, we show that diverse myosin II isoforms self-organize contractile units within bundles of F-actin and myosin thick filaments. Despite this minimal composition, along with the lack of regulation of F-actin length, organization, and polarity, these contractile units are biophysically analogous to sarcomeres that are present in striated muscle with a well-defined force-velocity relationship, length, and structure. The contractile units lack a clear structural organization, and emerge from local actomyosin interactions, providing insight into the minimal requirements to form contractile units in vivo. Interestingly, the maximal shortening rates

we measure in reconstituted bundles are strikingly similar to those observed in skeletal muscle ($1-2 \text{ s}^{-1}$), smooth muscle ($0.02-0.25 \text{ s}^{-1}$) (31,32), and nonmuscle ($0.004-0.08 \text{ s}^{-1}$) (33) cells. This indicates that these minimal self-organized contractile units reconstituted in vitro have similar lengths and shortening velocities to those in vivo and suggests that thick filament-mediated self-organization of contractile units may dominate the formation of contractile units in these more complex cytoskeletal arrays found in diverse cell types in vivo, even those with highly organized actomyosin.

Our data show that a reduced density of larger thick filaments promotes contraction. This supports our recently developed model of F-actin-buckling-induced actomyosin self-organization (20). In the model, stochastic variations in myosin thick filament speed result in randomly distributed compressive and tensile forces on portions of F-actin (Fig. 5). If these forces are sufficiently large, compressed F-actin buckle and collapse, whereas extended regions stay undeformed. (F-actin can withstand $>100 \text{ pN}$ of tensile force (34) but buckles readily over $1 \mu\text{m}$ length scales with $<1 \text{ pN}$ of compressive stress.) Thus, the random compressive stresses result in local bundle collapse, whereas tensile ones do not elicit deformation. Due to these local deformations, the bundle as a whole contracts. The average distance between buckles then becomes the effective contractile unit length ℓ_0 (Fig. 5).

To understand what sets this distance, we must note that as the thick filament length is increased, each of them exerts a larger local force on the F-actin. Moreover, if the total number of myosin heads is constant, the thick filaments are further apart; this results in a loosely cross-linked bundle, which is thus more prone to buckling. The combination of these two effects implies that buckling is more frequent when the length of the thick filament is increased (Fig. 5). As a consequence, the average distance between two buckles is shortened, and the contractile unit length is smaller. Thus, the number of motor heads plays a crucial role in determining the length scale of contractile units formed. This may play an especially important role in the regulation of smooth muscle contraction, where the thick filament length can be dynamically regulated (35,36).

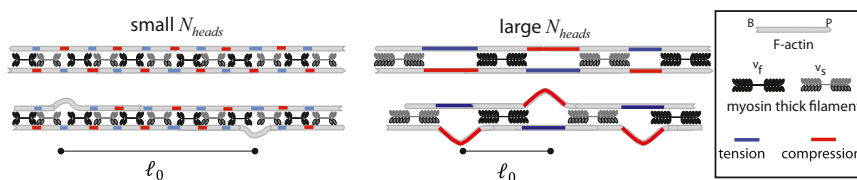


FIGURE 5 Cartoon model illustrating relationship between the number of heads per thick filament, N_{heads} , to the characteristic length of contractile units, ℓ_0 . This schematic summarizes the main findings of our theoretical model for contraction in disordered actomyosin bundles described in (20) as applied to this data. Myosin thick filaments drive sliding of antiparallel F-actin

(polar lines with barbed (B) and pointed (P) ends indicated). Stochastic effects cause a dispersion in thick filament motor speed at any given point in time, with portions of F-actin flanked between faster motors (v_f , black) and slower motors (v_s , gray) under either local tension (blue, faster filaments moving away from slower filaments) or compression (red, faster filaments moving toward slower filaments) within F-actin filaments. Above a critical force, compressive forces result in buckling of F-actin portions and facilitate local bundle contraction. Bundles composed of filaments with small N_{heads} (left) cross-link the F-actin to a greater extent and generate lower stresses on F-actin portions; both of these effects result in a lower frequency of buckling as compared to bundles formed with dilute densities of large thick filaments (right) and, thus, possess a larger characteristic contractile unit length scale.

After the self-organization process, we find that the properties of the contractile unit are consistent with those created by a bipolar thick filament acting on antiparallel F-actin. At initial times, there is little internal friction within the bundle such that the shortening velocity is determined by the unloaded gliding speed of the motor isoform and the maximum tension is determined by the number of motor heads acting in parallel on F-actin, determined by the thick filament length. Thus, the self-organization tends to build contractile units that act as functional sarcomeres within a disordered actin bundle. However, because these contractile units are stochastic and dynamic, self-organized contractile units are not limited by the same geometrical constraints as sarcomeres and contractility can be dynamically regulated by perturbations to thick filament length.

Although our understanding of contractility in striated muscle has benefited from the presence of highly organized sarcomeric contractile units (8), the regulation of contraction in nonmuscle and smooth muscle cells is not well understood. Our data show that, diverse isoforms of myosin II self-organize contractile units within bundles and that the thick filament length and motor mechanochemistry collaborate to build self-organized contractile units with distinct lengths, shortening velocities, and forces. These data provide insight into the regulation of contraction in disordered actomyosin bundles found in nonmuscle and smooth muscle cells.

SUPPORTING MATERIAL

Six supplemental figures as well as two movies and their legends, are available at [http://www.biophysj.org/biophysj/supplemental/S0006-3495\(12\)05176-4](http://www.biophysj.org/biophysj/supplemental/S0006-3495(12)05176-4).

MLG gratefully acknowledges support from the Packard Foundation and Burroughs Wellcome Fund Career Award. Work was supported by the NSF Materials Science and Engineering Consortium at the University of Chicago.

REFERENCES

- Vicente-Manzanares, M., X. Ma, ..., A. R. Horwitz. 2009. Non-muscle myosin II takes centre stage in cell adhesion and migration. *Nat. Rev. Mol. Cell Biol.* 10:778–790.
- Gardel, M. L., I. C. Schneider, ..., C. M. Waterman. 2010. Mechanical integration of actin and adhesion dynamics in cell migration. *Annu. Rev. Cell Dev. Biol.* 26: 3.1–3.19.
- Matsumura, F. 2005. Regulation of myosin II during cytokinesis in higher eukaryotes. *Trends Cell Biol.* 15:371–377.
- Carvalho, A., A. Desai, and K. Oegema. 2009. Structural memory in the contractile ring makes the duration of cytokinesis independent of cell size. *Cell.* 137:926–937.
- Gordon, A. M., E. Homsher, and M. Regnier. 2000. Regulation of contraction in striated muscle. *Physiol. Rev.* 80:853–924.
- Löfgren, M., U. Malmqvist, and A. Arner. 2001. Substrate and product dependence of force and shortening in fast and slow smooth muscle. *J. Gen. Physiol.* 117:407–418.
- Lecuit, T., P. F. Lenne, and E. Munro. 2011. Force generation, transmission, and integration during cell and tissue morphogenesis. *Annu. Rev. Cell Dev. Biol.* 27:157–184.
- Huxley, A. F. 1957. Muscle structure and theories of contraction. *Prog. Biophys. Biophys. Chem.* 7:255–318.
- Sweeney, H. L., and A. Houdusse. 2010. Structural and functional insights into the Myosin motor mechanism. *Annu. Rev. Biophys.* 39:539–557.
- Edman, K. A. 1979. The velocity of unloaded shortening and its relation to sarcomere length and isometric force in vertebrate muscle fibres. *J. Physiol.* 291:143–159.
- Herrera, A. M., B. E. McParland, ..., C. Y. Seow. 2005. ‘Sarcomeres’ of smooth muscle: functional characteristics and ultrastructural evidence. *J. Cell Sci.* 118:2381–2392.
- Hai, C. M., and R. A. Murphy. 1988. Regulation of shortening velocity by cross-bridge phosphorylation in smooth muscle. *Am. J. Physiol.* 255:C86–C94.
- Malmqvist, U., and A. Arner. 1991. Correlation between isoform composition of the 17 kDa myosin light chain and maximal shortening velocity in smooth muscle. *Pflugers Arch.* 418:523–530.
- Tanner, K., A. Boudreau, ..., S. Kumar. 2010. Dissecting regional variations in stress fiber mechanics in living cells with laser nanosurgery. *Biophys. J.* 99:2775–2783.
- Katoh, K., Y. Kano, ..., K. Fujiwara. 1998. Isolation and contraction of the stress fiber. *Mol. Biol. Cell.* 9:1919–1938.
- Bárány, M. 1967. ATPase activity of myosin correlated with speed of muscle shortening. *J. Gen. Physiol.* 50(Suppl. 6):197–218.
- Ijima, G., A. M. Al-Jumaily, ..., G. C. Sieck. 2011. Myosin filament polymerization and depolymerization in a model of partial length adaptation in airway smooth muscle. *J. Appl. Physiol.* 111:735–742.
- Seow, C. Y. 2005. Myosin filament assembly in an ever-changing myofilament lattice of smooth muscle. *Am. J. Physiol. Cell Physiol.* 289:C1363–C1368.
- Thoresen, T., M. Lenz, and M. L. Gardel. 2011. Reconstitution of contractile actomyosin bundles. *Biophys. J.* 100:2698–2705.
- Lenz, M., T. Thoresen, ..., A. R. Dinner. 2012. Contractile units in disordered actomyosin bundles arise from F-actin buckling. *Phys. Rev. Lett.* 108:238107.
- Adelstein, R. S., and C. B. Klee. 1981. Purification and characterization of smooth muscle myosin light chain kinase. *J. Biol. Chem.* 256:7501–7509.
- Kovar, D. R., J. R. Kuhn, ..., T. D. Pollard. 2003. The fission yeast cytokinesis formin Cdc12p is a barbed end actin filament capping protein gated by profilin. *J. Cell Biol.* 161:875–887.
- Skubiszak, L., and L. Kowalczyk. 2002. Myosin molecule packing within the vertebrate skeletal muscle thick filaments. A complete bipolar model. *Acta Biochim. Pol.* 49:829–840.
- Aratyn-Schaus, Y., P. W. Oakes, ..., M. L. Gardel. 2010. Preparation of complaint matrices for quantifying cellular contraction. *J. Vis. Exp.* 14:46.
- Yeung, T., P. C. Georges, ..., P. A. Janmey. 2005. Effects of substrate stiffness on cell morphology, cytoskeletal structure, and adhesion. *Cell Motil. Cytoskeleton.* 60:24–34.
- Craig, R., and J. Megerman. 1977. Assembly of smooth muscle myosin into side-polar filaments. *J. Cell Biol.* 75:990–996.
- Niederman, R., and T. D. Pollard. 1975. Human platelet myosin. II. In vitro assembly and structure of myosin filaments. *J. Cell Biol.* 67:72–92.
- Rovner, A. S., P. M. Fagnant, ..., K. M. Trybus. 2002. The carboxyl-terminal isoforms of smooth muscle myosin heavy chain determine thick filament assembly properties. *J. Cell Biol.* 156:113–123.
- Huxley, H. E. 1963. Electron microscope studies on the structure of natural and synthetic protein filaments from striated muscle. *J. Mol. Biol.* 7:281–308.

30. Achim, B., and S. S. Ulrich. 2007. Coupling biochemistry and mechanics in cell adhesion: a model for inhomogeneous stress fiber contraction. *New J. Phys.* 9:425.
31. Draeger, A., W. B. Amos, ..., J. V. Small. 1990. The cytoskeletal and contractile apparatus of smooth muscle: contraction bands and segmentation of the contractile elements. *J. Cell Biol.* 111:2463–2473.
32. Gerthoffer, W. T. 1991. Regulation of the contractile element of airway smooth muscle. *Am. J. Physiol.* 261:L15–L28.
33. Russell, R. J., S. L. Xia, ..., T. P. Lele. 2009. Sarcomere mechanics in capillary endothelial cells. *Biophys. J.* 97:1578–1585.
34. Kishino, A., and T. Yanagida. 1988. Force measurements by micro-manipulation of a single actin filament by glass needles. *Nature.* 334:74–76.
35. Ashton, F. T., A. V. Somlyo, and A. P. Somlyo. 1975. The contractile apparatus of vascular smooth muscle: intermediate high voltage stereo electron microscopy. *J. Mol. Biol.* 98:17–29.
36. Seow, C. Y., V. R. Pratushevich, and L. E. Ford. 2000. Series-to-parallel transition in the filament lattice of airway smooth muscle. *J. Appl. Physiol.* 89:869–876.
37. Cuda, G., E. Pate, ..., J. R. Sellers. 1997. In vitro actin filament sliding velocities produced by mixtures of different types of myosin. *Biophys. J.* 72:1767–1779.
38. Umemoto, S., and J. R. Sellers. 1990. Characterization of in vitro motility assays using smooth muscle and cytoplasmic myosins. *J. Biol. Chem.* 265:14864–14869.
39. Harris, D. E., and D. M. Warshaw. 1993. Smooth and skeletal muscle myosin both exhibit low duty cycles at zero load in vitro. *J. Biol. Chem.* 268:14764–14768.
40. Tyska, M. J., D. E. Dupuis, ..., S. Lowey. 1999. Two heads of myosin are better than one for generating force and motion. *Proc. Natl. Acad. Sci. USA.* 96:4402–4407.
41. Molloy, J. E., J. E. Burns, ..., D. C. White. 1995. Movement and force produced by a single myosin head. *Nature.* 378:209–212.
42. Sobieszek, A. 1972. Cross-bridges on self-assembled smooth muscle myosin filaments. *J. Mol. Biol.* 70:741–744.
43. Tonino, P., M. Simon, and R. Craig. 2002. Mass determination of native smooth muscle myosin filaments by scanning transmission electron microscopy. *J. Mol. Biol.* 318:999–1007.